

Colour corrections for high redshift objects due to intergalactic attenuation

Avery Meiksin

*SUPA**, *Institute for Astronomy, University of Edinburgh, Blackford Hill, Edinburgh EH9 3HJ, UK*

18 June 2018

ABSTRACT

Corrections to the magnitudes of high redshift objects due to intergalactic attenuation are computed using current estimates of the properties of the intergalactic medium. The results of numerical simulations are used to estimate the contributions to resonant scattering from the higher order Lyman transitions. Differences of 0.5 – 1 magnitude from the previous estimate of Madau (1995) are found. Intergalactic k_{IGM} -corrections and colours are provided for high redshift starburst galaxies and Type I and Type II QSOs for several filter systems used in current and planned deep optical and infra-red surveys.

Key words: galaxies: high redshift - galaxies: photometry - intergalactic medium - quasars: absorption lines - quasars: general - surveys

1 INTRODUCTION

Over the past decade, deep optical and infra-red surveys have enabled giant strides to be taken in elucidating the nature and properties of objects that populate the high redshift universe. The band-dropout method has unveiled a population of Lyman break galaxies at $z \approx 3$ (Guhathakurta et al. 1990; Bithell 1991; Steidel & Hamilton 1992, 1993; Steidel, Pettini & Hamilton 1995; Steidel et al. 2003) and higher (Sawicki & Thompson 2005). The selection method was successfully applied to the Hubble Deep Field (HDF) (Giavalisco, Steidel & Macchetto 1996; Steidel et al. 1996), broadening the redshift range and volume coverage over previous surveys. Most recently the Ultra Deep Field (UDF) was exploited to discover objects as distant as $z \gtrsim 6$ (Stanway, Bunker & McMahon 2003; Bouwens et al. 2004; Yan & Windhorst 2004; Giavalisco et al. 2004).

An alternative selection method for identifying high redshift objects relies on combinations of broadband colours to estimate photometric redshifts, for which the most likely redshift is assigned based on predicted spectral energy distributions (Sawicki, Lin & Yee 1997; Csabai et al. 2000).

The modelling of the high redshift objects through population synthesis, applied to a combination of spectroscopic data and broad-band colours, suggests that most of the high redshift objects are star-forming galaxies (Madau et al. 1996; Metcalfe et al. 2001; Papovich, Dickinson & Ferguson 2001; Pettini et al. 2001; Shapley et al. 2003). A few of the Lyman break galaxies contain Active Galactic Nuclei

(Steidel et al. 2002), used to determine the faint end of the QSO luminosity function at $z \approx 3$ (Hunt et al. 2004).

Parallel to these surveys have been several searches for high redshift Quasi-Stellar Objects (QSOs). The discovery of a few dozen $z > 3.6$ QSOs by the Sloan Digital Sky Survey (SDSS) has made possible a new evaluation of the bright end of the QSO luminosity function and its evolution at these high redshifts (Fan et al. 2001). The results are currently being revised (Richards et al. 2005) based on the much larger numbers now detected, including over 500 at $z > 4$ (Schneider et al. 2005).

Similar surveys are expected to continue well into the future, including some now in progress, such as the Canada-France-Hawaii Telescope Legacy Survey (CFHTLS[†]) and the UKIRT Infrared Deep Sky Survey (UKIDSS[‡]; Hewett et al. , in preparation), or planned for telescopes currently under development, such as the Visible & Infrared Survey Telescope for Astronomy (VISTA[§]) and the *James Webb Space Telescope* (JWST[¶]).

Crucial to all these analyses is an accurate estimate of the amount of intergalactic attenuation due to intervening absorption systems. Most have relied on the standard work of Madau (1995), whose assessment was based on the then most current understanding of the properties and distributions of intervening systems. Madau (1995) estimated the

[†] www.cfht.hawaii.edu/Science/CFHLS/

[‡] www.ukidss.org

[§] www.vista.ac.uk

[¶] www.ngst.nasa.gov

* Scottish Universities Physics Alliance

blanketing due to the resonant (Lyman series) scattering of photons assuming idealised forms for the H I column density distribution of the absorbers. The contributions of the different orders in the Lyman series depend on the full line-shape of the absorber, precluding a direct scaling of line-centre optical depths based on pure atomic physics considerations. Instead the broadening of the absorbers must be included, the distribution of which has since been shown to be sensitive to column density (Kirkman & Tytler 1997; Kim, Cristiani & D’Odorico 2002b). Madau (1995) adopted a constant Doppler parameter for all absorption systems, varying the value to probe the sensitivity of the total amount of attenuation to this variable. A blanketing formalism based on Poisson placement of the absorbers was used to predict the effective optical depths, although in principle small scale clustering of the absorption systems will affect the total amount of blanketing, and such correlations have been detected (Kirkman & Tytler 1997; Kim et al. 2002a).

Since Madau’s seminal work, numerical simulations of the intergalactic medium have yielded results matching the measured distributions of the Ly α flux distributions to an accuracy of a few percent, as well as the line parameters (allowing for extra heating) (Meiksin, Bryan & Machacek 2001). Numerical simulations have also reproduced the H I column density dependence of the Doppler parameter envelope (Misawa et al. 2004), as well as correlations in the H I flux distribution (Croft et al. 2002; Meiksin & White 2004). The understanding of the mean Ly α intergalactic optical depths has improved substantially over the past decade (see Meiksin & White 2004 for a summary and Kirkman et al. 2005 for subsequent results). The simulations contain the information necessary to extract the contributions from all higher order transitions to the blanketing. Although simulations do not recover the full numbers of Lyman Limit Systems observed (Gardner et al. 1997; Meiksin & White 2004), an assessment of their numbers over the redshift range $0.3 \lesssim z \lesssim 4$ has been made by Stengler-Larrea et al. (1995). These improvements now permit a much more secure determination of the amount of intergalactic attenuation to be made.

2 NUMERICAL SIMULATION PREDICTIONS FOR INTERGALACTIC ATTENUATION

Attenuation due to intervening intergalactic hydrogen arises through two principle mechanisms, resonant scattering by Lyman transitions and photoelectric absorption. Additional contributions are made by intervening metal systems and intervening helium. The contributions of metals and He I are small (Madau 1995), while He II will contribute only at wavelengths $\lambda < 228(1+z)\text{\AA}$ for a source at redshift z .

The hydrogen attenuation values are based on the simulation of a Λ CDM model by Meiksin & White (2004) with $\Omega_M = 0.3$, $\Omega_b = 0.7$, $h = 0.7$, $n = 0.95$, and normalised to $\sigma_8 = 0.92$, consistent with *WMAP* constraints. The simulation used a pure particle mesh (PM) scheme (Meiksin & White 2001), mimicking the temperature of the gas using a polytropic equation of state and assuming the gas and dark matter have the same spatial distribution. The mean transmitted Ly α fluxes are normalised using the values listed in Table 3 of Meiksin & White (2004). The attenuation values

Table 1. Ratio of $\bar{\tau}_n/\bar{\tau}_\alpha$ for Lyman transition $n \rightarrow 1$ for $n = 3$ to 9. Each transition contributes at wavelength λ for an object at redshift z only under the condition $z_n < z$, where $z_n \equiv (\lambda/\lambda_n) - 1$ and λ_n is the (rest) wavelength of the transition.

n	$\bar{\tau}_n/\bar{\tau}_\alpha$
3	$0.348[0.25(1+z_n)]^{1/3}, (z_n < 3); 0.348[0.25(1+z_n)]^{1/6}, (z_n > 3)$
4	$0.179[0.25(1+z_n)]^{1/3}, (z_n < 3); 0.179[0.25(1+z_n)]^{1/6}, (z_n > 3)$
5	$0.109[0.25(1+z_n)]^{1/3}, (z_n < 3); 0.109[0.25(1+z_n)]^{1/6}, (z_n > 3)$
6	$0.0722[0.25(1+z_n)]^{1/3}$
7	$0.0508[0.25(1+z_n)]^{1/3}$
8	$0.0373[0.25(1+z_n)]^{1/3}$
9	$0.0283[0.25(1+z_n)]^{1/3}$

resulting from higher order Lyman transitions are computed directly from the simulation results.

The mean optical depth value for the Lyman transition $n \rightarrow 1$ is defined by

$$\bar{\tau}_n \equiv -\ln\langle\exp(-\tau_n)\rangle, \quad (1)$$

where $\langle\exp(-\tau_n)\rangle$ is the corresponding mean transmitted flux. (Here, the convention $\tau_\alpha = \tau_2$, $\tau_\beta = \tau_3$, etc. will be adopted.) For $2 < z < 4$, the measured values of the mean Ly α transmitted flux are fit to within 2% using

$$\bar{\tau}_\alpha = 0.00211(1+z)^{3.7} \quad (z < 4). \quad (2)$$

The sharp reduction in flux at higher redshifts is adequately fit by

$$\bar{\tau}_\alpha = 0.00058(1+z)^{4.5} \quad (z > 4). \quad (3)$$

For $z > 6$, the measured values become quite uncertain, but the objects become dimmed by 4 magnitudes or more so that accurate values will normally not be required.

The higher order terms in the Lyman series are characterised by the ratio $\bar{\tau}_n/\bar{\tau}_\alpha$ to factor out most of the redshift dependence. A residual dependence, however, remains. These are accurately fit (to within a few percent) by weak powers of $(1+z)$. The ratios for the first 7 orders (Ly β to Ly θ) after Ly α are provided in Table 1. Higher orders ($n > 9$) are found to scale very nearly according to the atomic physics prediction for line-centre optical depth values:

$$\frac{\bar{\tau}_n}{\bar{\tau}_\theta} \approx \frac{720}{n(n^2-1)}. \quad (4)$$

Terms up to $n = 31$ are included: higher order Lyman series transitions contribute negligibly.

The contribution due to photoelectric absorption is split into two parts, the contribution from systems optically thin at the Lyman edge and the contribution from Lyman Limit Systems. The contribution from optically thin systems is given in the linear approximation $\tau_L = r/r_0$ (Zuo 1992), where r is the proper distance between the emitting object at redshift z and the redshift $z_L = \lambda/\lambda_L - 1$, where λ_L is the wavelength at the Lyman edge ($\lambda_L = 912\text{\AA}$), λ is the observed wavelength, and r_0 is the attenuation length of photons at the photoelectric edge. Using the result for the attenuation length from Meiksin & White (2004), this is well-approximated by

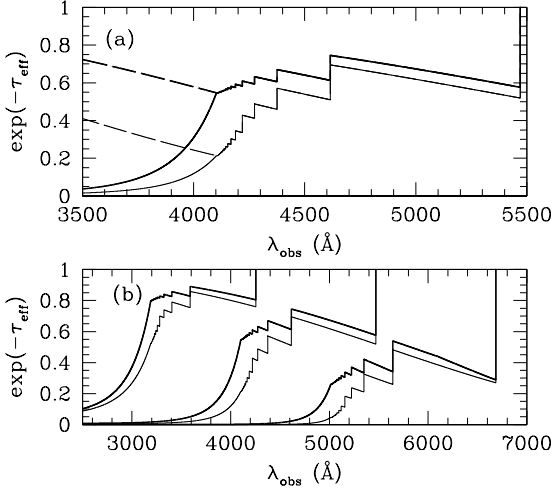


Figure 1. Intergalactic transmission as a function of observed wavelength. (a) Mean intergalactic transmission for a source at redshift $z = 3.5$ (solid lines). The mean intergalactic transmission assuming no Lyman Limit Systems lie along the line-of-sight is shown by the dashed lines. (b) Mean intergalactic transmission for, from left to right, sources at redshifts $z = 2.5, 3.5$ and 4.5 . The heavy lines are the estimates from this paper. In both panels, the light lines are the estimates from Madau (1995).

$$\tau_L^{\text{IGM}} = 0.805(1 + z_L)^3 \left(\frac{1}{1 + z_L} - \frac{1}{1 + z} \right). \quad (5)$$

The contribution due to Poisson-distributed Lyman Limit Systems is given by (Zuo 1992)

$$\tau_L^{\text{LLS}} = \int_{z_L}^z dz' \int_1^\infty d\tau_L \frac{\partial^2 N}{\partial \tau_L \partial z'} \left\{ 1 - \exp \left[-\tau_L \left(\frac{1 + z_L}{1 + z'} \right)^3 \right] \right\}, \quad (6)$$

where $\partial^2 N / \partial \tau_L \partial z = A \tau_L^{-\beta} (1 + z)^\gamma$ is assumed, corresponding to a number density $dN/dz = N_0 (1 + z)^\gamma$ for systems with $\tau_L > 1$, where $N_0 = A / (\beta - 1)$. The integral has the power series solution

$$\begin{aligned} \tau_L^{\text{LLS}} = & \frac{N_0}{4 + \gamma - 3\beta} \left[\Gamma(2 - \beta, 1) - e^{-1} - \sum_{n=0}^{\infty} \frac{\beta-1}{n+1-\beta} \frac{(-1)^n}{n!} \right] \\ & \times \left[(1 + z)^{-3(\beta-1) + \gamma + 1} \left(\frac{\lambda}{\lambda_L} \right)^{3(\beta-1)} - \left(\frac{\lambda}{\lambda_L} \right)^{\gamma+1} \right] \\ & - N_0 \sum_{n=1}^{\infty} \frac{\beta-1}{(3n-\gamma-1)(n+1-\beta)} \frac{(-1)^n}{n!} \\ & \times \left[(1 + z)^{\gamma+1-3n} \left(\frac{\lambda}{\lambda_L} \right)^{3n} - \left(\frac{\lambda}{\lambda_L} \right)^{\gamma+1} \right]. \quad (7) \end{aligned}$$

The first 10 terms of each series provide a high level of convergence. The results are normalised to $N_0 = 0.25$, $\beta = 1.5$ and $\gamma = 1.5$ (Stengler-Larrea et al. 1995). Although the result of Stengler-Larrea et al. applies only for $z \lesssim 4$, the redshift dependence is extrapolated to higher redshifts here, noting that the contribution of these systems is uncertain at these redshifts.

The total optical depth is the sum of the resonant and photoelectric contributions. The photoelectric contribution is dominated by systems with $\tau_L \approx 1$; optically thin systems

contribute only a small amount while very optically thick systems are too few in number to contribute much on average. While the photoelectric contribution due to the optically thin IGM is well-determined due to the large number of optically thin systems, the contribution from Lyman Limit Systems is highly variable, depending on the chance that a Lyman Limit System lies along the relevant path length. For instance, for a source at $z = 3.5$, the Lyman limit lies at the observed wavelength $\lambda = 4104 \text{ \AA}$. The number of Lyman Limit Systems that will fall at a redshift corresponding to the U_n -band wavelength range of approximately $3000 \text{ \AA} - 4000 \text{ \AA}$ is 2.1. The Poisson probability that no Lyman Limit System lies in this range is then $e^{-2.1} = 0.12$. This will introduce large fluctuations in the amount of attenuation at these short wavelengths (Zuo & Phinney 1993; Madau 1995), a fact which should be borne in mind when interpreting the number of source detections in Lyman dropout surveys.

An indication of the level of contribution of Lyman Limit Systems to the total optical depth is provided in Figure 1a, which shows the level of intergalactic transmission as a function of observed wavelength and the transmission with the contribution of Lyman Limit Systems removed. The total intergalactic transmissions allowing for H I attenuation are shown as a function of the observed wavelength for sources at $z = 2.5, 3.5$ and 4.5 in Figure 1b, and in Table 2. The figures include comparisons with the corresponding estimates of Madau (1995), which tend to lower transmission levels, primarily as a result of differences in the estimates of the contributions of resonant absorption.

3 EFFECT OF INTERGALACTIC ATTENUATION ON BROADBAND MAGNITUDES

In the AB-magnitude system, the apparent magnitude of a source of intrinsic flux f_ν (in cgs units) measured through a filter with (normalised) transmissivity $T(\nu)$ is given by

$$m_{AB} = -2.5 \log_{10} \int d\nu f_\nu \exp(-\tau_{\text{eff}}) T(\nu) - 48.59. \quad (8)$$

The difference between the magnitudes with and without intergalactic attenuation will be designated as the intergalactic k-correction $k_{\text{IGM}} = m_{AB}(\tau_{\text{eff}}) - m_{AB}(\tau_{\text{eff}} = 0)$. Because source spectra are typically slowly varying over a bandwidth, the k_{IGM} -correction is fairly independent of the nature of the source. The exception is when either the source has narrow features that dominate the light, such as strong emission or absorption lines, or when the amount of intergalactic attenuation varies rapidly within a band, reducing the wavelength range of the source spectrum that contributes to the total magnitude, and so enhancing the effect of any differences between source spectra.

To indicate the typical role intergalactic attenuation plays on the colours of high redshift objects, the effect of intergalactic attenuation is evaluated for four model sources: starbursts of ages 3 Myr and 600 Myr, roughly bracketing the range inferred for Lyman Break Galaxies (Papovich, Dickinson & Ferguson 2001), and Type I and Type II QSOs. The starburst spectra assume continuous star formation with solar metallicity and a Salpeter Initial Mass

Table 2. Intergalactic H I transmission as a function of observed wavelength.

λ (Å)	$z = 1.5$	$z = 2.0$	$z = 2.5$	$z = 3.0$	$z = 3.5$	$z = 4.0$	$z = 4.5$	$z = 5.0$	$z = 5.5$	$z = 6.0$	$z = 6.5$	$z = 7.0$
1730.0	0.323241	0.150055	0.074558	0.038532	0.020407	0.010983	0.005976	0.003277	0.001807	0.001001	0.000556	0.000310
1731.0	0.323538	0.150066	0.074510	0.038482	0.020369	0.010956	0.005958	0.003266	0.001800	0.000996	0.000553	0.000308
1732.0	0.323836	0.150077	0.074462	0.038433	0.020330	0.010929	0.005940	0.003254	0.001793	0.000992	0.000550	0.000306
1733.0	0.324135	0.150089	0.074414	0.038383	0.020292	0.010902	0.005922	0.003243	0.001785	0.000987	0.000548	0.000304
1734.0	0.324436	0.150101	0.074367	0.038334	0.020253	0.010875	0.005905	0.003231	0.001778	0.000983	0.000545	0.000303

Note: The full table is published in the electronic version of the paper. A portion is shown here only for guidance regarding its form and content.

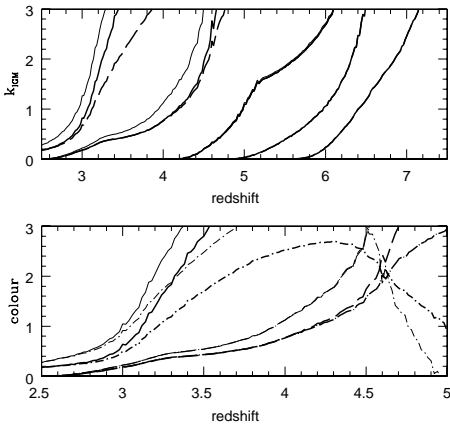


Figure 2. Intergalactic attenuation k_{IGM} -correction and colours for a 600 Myr starburst with continuous star formation. (a) From left to right, k_{IGM} for U_n , G , \mathcal{R} , I and z' bands (solid lines). For the U_n and G bands, k_{IGM} assuming the absence of Lyman Limit Systems is shown by the dashed lines. The absence of Lyman Limit Systems leaves the results for the remaining bands unaltered. The light solid lines correspond to the predictions for k_{IGM} using the attenuation model of Madau (1995). (b) The $U_n - G$ (solid) and $G - \mathcal{R}$ (long dashed) colours of the starburst. The dotted short-dashed lines and dotted long-dashed line show $U_n - G$ and $G - \mathcal{R}$, respectively, assuming the absence of Lyman Limit Systems. The light lines correspond to the predictions based on the attenuation model of Madau (1995).

Function and were generated by the STARBURST99 model of Leitherer et al. (1999). The Type I QSO spectrum is the composite spectrum constructed from over 2200 spectra homogeneously selected from the SDSS QSO survey covering the redshift interval $0.044 < z < 4.789$ and restframe wavelength range $800\text{\AA} - 8555\text{\AA}$ (Vanden Berk et al. 2001). The Type II QSO spectrum is based on observations of CXO 52 (Stern et al. 2002), as described in Meiksin (2005). This Type II QSO was chosen because it has high equivalent width emission lines that will dominate the magnitude of the band in which they lie, and so represents a class of objects that will have unusual broadband colours that vary substantially with redshift.

The effect of intergalactic attenuation on broadband magnitudes is computed for several filter systems relevant to recent and planned major surveys: the Sloan $u'g'r'i'z'$ system (assuming airmass 1.3 response for a point source); the $U_n\mathcal{GR}$ system of Steidel's group, supplemented by the I -band adopting the Harris I filter; the *Hubble Space Telescope* (HST) ACS/NICMOS B_{435} ($F435W$), V_{606} ($F606W$), i_{775} ($F775W$), z_{850} ($F850LP$), J_{110} ($F110W$) and H_{160} ($F160W$) bands (including instrumental responses); the UKIDSS $ZYJHK$ filters; and the *JWST* $F070W$ (designated m_{070} and approximated as a square transmission response) and $F150W$ (designated m_{150}) bands. All magnitudes are computed on the AB system.

The k_{IGM} -corrections and colours for the U_n , G and \mathcal{R} filters of Steidel & Hamilton (1992) as well as the I and z' bands, are shown in Figure 2 for the 600 Myr old starburst. The effect of internal reddening is not included. This will negligibly affect k_{IGM} , so the magnitude corrections to the colours due to reddening will simply be additive. Also shown are the results assuming no Lyman Limit Systems intercept the line-of-sight. The mean contribution of Lyman Limit Systems has a substantial effect on U_n , a small effect on G , and a negligible effect on the longer wavelength bands for $k_{IGM} < 3$. A comparison with the attenuation model of Madau (1995) shows a reduction in k_{IGM} of about 0.5 magnitude, although the effect on the colours approach a shift of a full magnitude. In terms of photometric redshifts, the difference in attenuation models produces a shift of $\Delta z = 0.1 - 0.2$ for $U_n - G$ and $G - \mathcal{R}$. The k_{IGM} -corrections and various colour combinations for all the sources considered are shown in Figures 3 and 4. The k_{IGM} -corrections are nearly independent of the source spectrum, except for the Type II QSO for which the magnitudes may be dominated by emission lines (Meiksin 2005). The colours also are similar except for the Type II QSO, although certain colours, such as UKIDSS $J - K$ and $H - K$, are particularly effective at separating the other sources.

4 SUMMARY

The amount of the attenuation of light from high redshift objects on passing through the IGM has been computed based on recent measurements of the mean transmitted Ly α flux through the IGM and recent assessments of the numbers of Lyman Limit Systems. The properties of the IGM required to compute the attenuation due to resonant Lyman photon scattering were based on numerical simulations matching the measured properties of the IGM. Differences from the predictions of the model of Madau (1995) are found for k_{IGM}

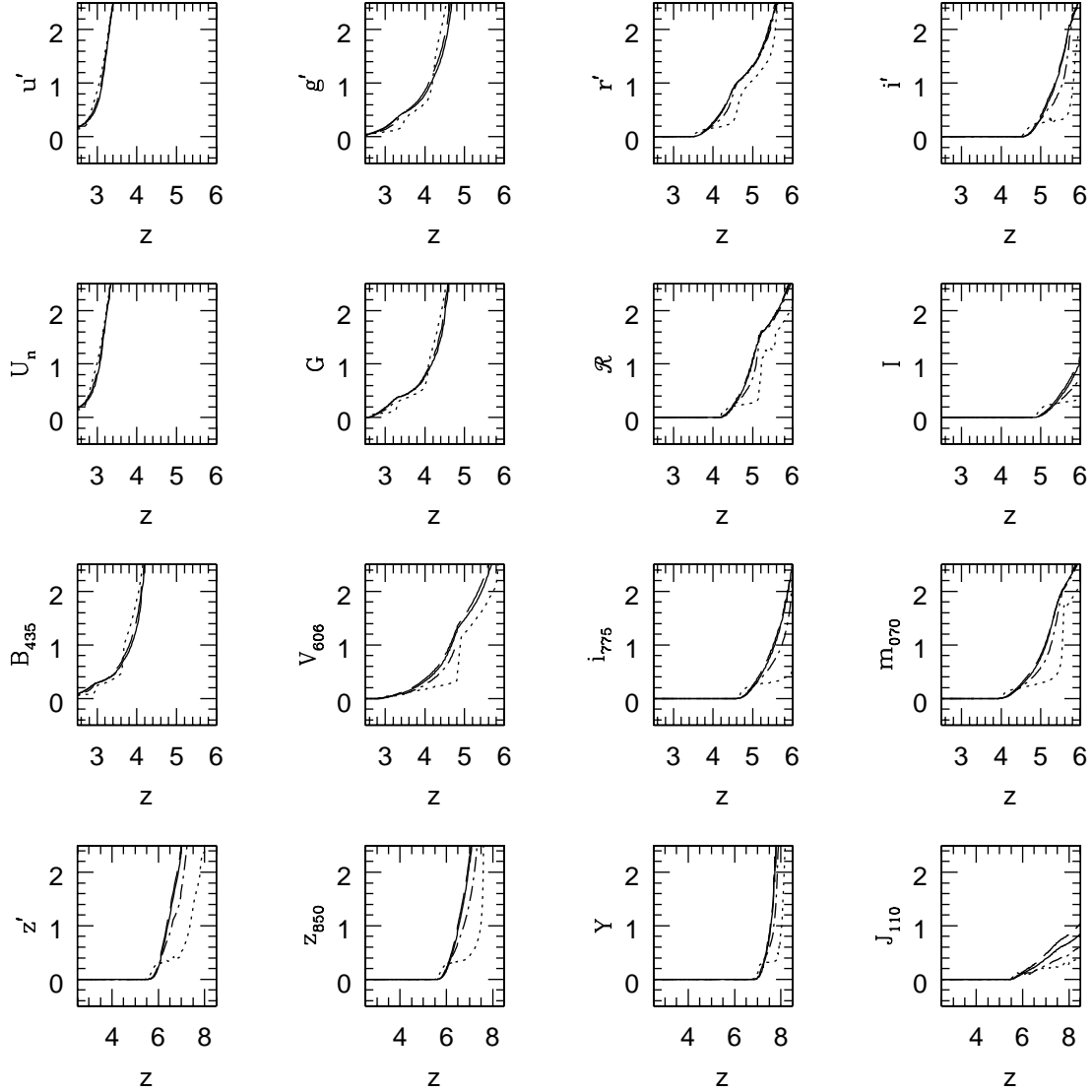


Figure 3. Intergalactic attenuation k_{IGM} -corrections as a function of source redshift for a 600 Myr starburst (solid lines), a 3 Myr starburst (long-dashed lines), a Type I QSO (dot-dashed lines) and a Type II QSO with high equivalent width emission lines (dotted lines). There is little variation between the sources except for the Type II QSO because of the presence of strong emission lines. The rows correspond to the following filter systems. First row: Sloan; second row: Steidel U_nGR filters and I -band; third row: HST bands B_{435} , V_{606} , i_{775} and $JWST$ m_{070} ; fourth row: Sloan z' , HST z_{850} and J_{110} and UKIDSS Y . The k_{IGM} -corrections are negligible for the HST H_{160} , $JWST$ m_{150} and UKIDSS J , H and K bands for $z < 8.5$.

and colours of 0.5 – 1 magnitude for bands containing rest-frame $\text{Ly}\alpha$ and shorter wavelengths.

Intergalactic k_{IGM} -corrections are provided for filter systems used in current or planned deep optical and infrared surveys, *viz.* the Sloan $u'g'r'i'z'$ system, Steidel U_nGR and the I -band, UKIDSS $ZYJHK$, the HST B_{435} , V_{606} , i_{775} , z_{850} , J_{110} and H_{160} bands, and the $JWST$ $F070W$ and $F150W$ bands.

Colours based on the above bands are provided for starbursts of ages 3 Myr and 600 Myr, typical of $z \approx 3$ Lyman Break Galaxies, and Type I and Type II QSOs, over the redshift range $2.5 < z < 8.5$. The results show which colours are most effective for distinguishing between different ob-

jects and the typical values to expect, which may be used for the planning and analysis of current and upcoming deep surveys.

ACKNOWLEDGMENTS

The author thanks Dr Steve Warren for kindly providing total response curves for the UKIDSS filter system.

REFERENCES

Bithell M., 1991, MNRAS, 253, 320

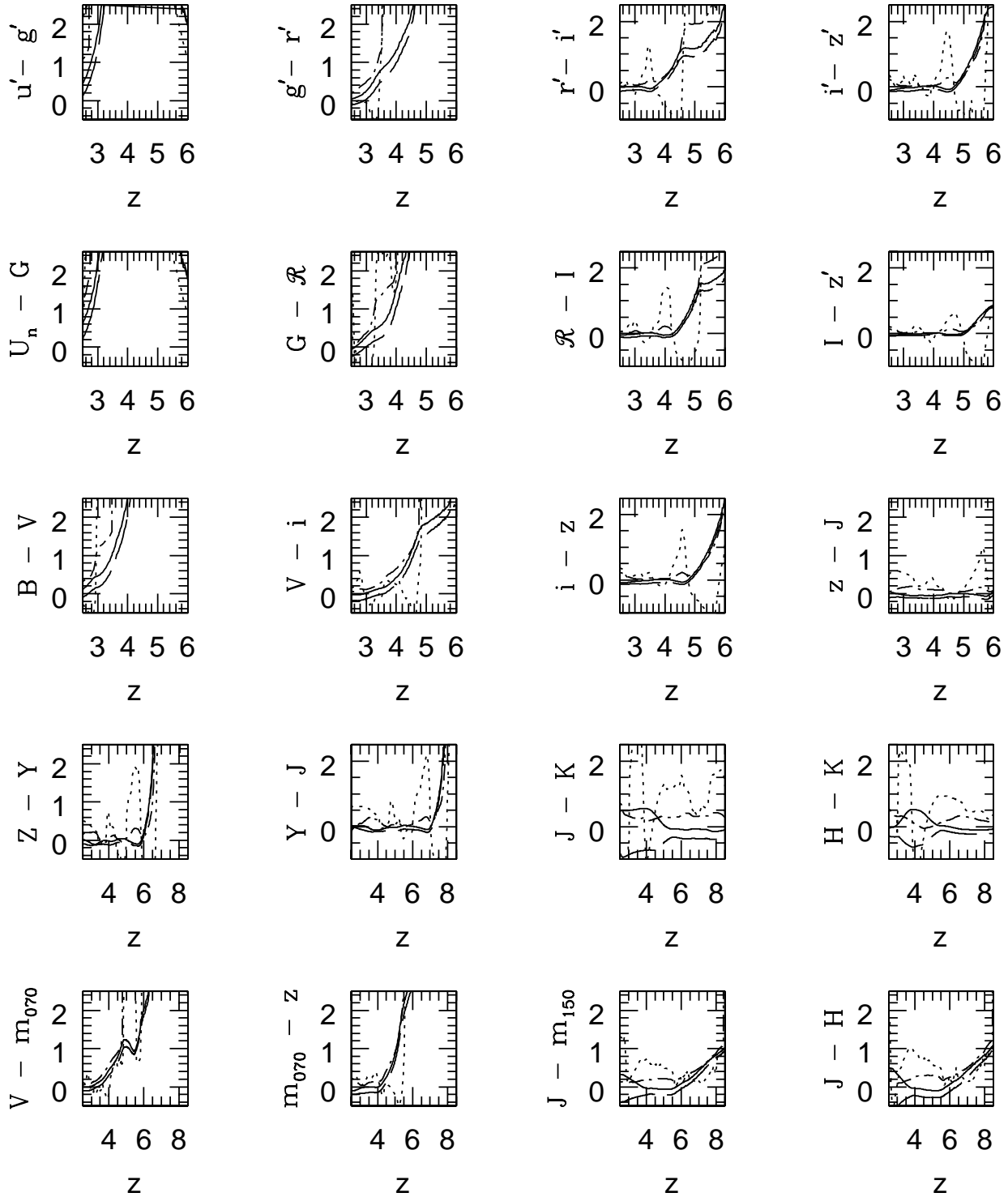


Figure 4. Colour predictions including the effects of intergalactic attenuation for a 600 Myr starburst (solid lines), a 3 Myr starburst (long-dashed lines), a Type I QSO (dot-dashed lines) and a Type II QSO with high equivalent width emission lines (dotted lines). In the third and fifth rows, the B , V , i , z , J and H magnitudes refer to the *HST* B_{435} , V_{606} , i_{775} , z_{850} , J_{110} and H_{160} bands, respectively. The fourth row magnitudes refer to the UKIDSS $ZYJHK$ bands.

- Bouwens R. J., Thompson R.I., Illingsworth G. D., Franx M., van Dokkum P., Fan X., Dickinson M. E., Eisenstein D. J., Rieke M. J., 2004, *ApJ*, 616, L79
- Croft R. A. C., Weinberg D. H., Bolte M., Burles S., Hernquist L., Katz N., Kirkman D., Tytler D., 2002, *ApJ*, 581, 20
- Csabai I., Connolly A. J., Szalay A. S., Budavári T., 2000, *AJ*, 119, 69
- Fan X., et al. , 2001, *AJ*, 121, 54
- Gardner J. P., Katz N., Hernquist L., Weinberg D. H., 1997, *ApJ*, 484, 31
- Giavalisco M., Steidel C. C., Macchetto F. D., 1996, *ApJ*, 470, 189
- Giavalisco M. et al. , 2004, *ApJ*, 600, L103
- Guhathakurta P., Tyson J. A., Majewski S. R., 1990, *ApJ*, 357, L9
- Kim T.-S., Carswell R. F., Cristiani S., D'Odorico S., Giallongo E., 2002a, *MNRAS*, 335, 555
- Kim T.-S., Cristiani S., D'Odorico S., 2002b, *A&A*, 383, 747
- Kirkman D., Tytler D., 1997, *ApJ*, 484, 672
- Kirkman D. et al., 2005, *MNRAS*, 360, 1373
- Hunt M. P., Steidel C. C., Adelberger K. L., Shapley A. E., 2004, *ApJ*, 605, 625
- Leitherer C. et al., 1999, *ApJS*, 123, 3
- Madau P., 1995, *ApJ*, 441, 18
- Madau P., Ferguson H. C., Dickinson M. E., Giavalisco M., Steidel C. C., Fruchter A., 1996, *MNRAS*, 283, 1388
- Meiksin A., 2005, *MNRAS*, in press
- Meiksin A., Bryan G. L., Machacek M. E., 2001, *MNRAS*, 327, 296
- Meiksin A., White M., 2001, *MNRAS*, 324, 141
- Meiksin A., White M., 2004, *MNRAS*, 350, 1107
- Metcalfe N., Shanks T., Campos A., McCracken H. J., Fong R., 2001, *MNRAS*, 323, 795
- Misawa T., Tytler D., Iye M., Paschos P., Norman M., Kirkman D., O'Meara J., Suzuki N., Kashikawa N., 2004, *AJ*, 128, 2954
- Papovich C., Dickinson M., Ferguson H. C., 2001, *ApJ*, 559, 620
- Pettini M., Shapley A. E., Steidel C. C., Cuby J.-G., Dickinson M., Moorwood A. F. M., Adelberger K. L., Giavalisco M., 2001, *ApJ*, 554, 981
- Sawicki M. J., Lin H., Yee H. K. C., 1997, *AJ*, 113, 1
- Sawicki M., Thompson D., 2005, *ApJ*, in press (astro-ph/0507424)
- Schneider D. P. et al., 2005, *AJ*, 130, 367
- Shapley A. E., Steidel C. C., Pettini M., Adelberger K. L., 2003, *ApJ*, 588, 65
- Stanway E. R., Bunker A. J., McMahon R. G., 2003, *MNRAS*, 342, 439
- Steidel C. C., Adelberger K. L., Shapley A. E., Pettini M., Dickinson M., Giavalisco M., 2003, *ApJ*, 592, 728
- Steidel C. C., Giavalisco M., Dickinson M., Adelberger K. L., 1996, *AJ*, 112, 352
- Steidel C. C., Hamilton D., 1992, *AJ*, 104, 941
- Steidel C. C., Hamilton D., 1993, *AJ*, 105, 2017
- Steidel C. C., Hunt M. P., Shapley A. E., Adelberger K. L., Pettini M., Dickinson M., Giavalisco M., 2002, *ApJ*, 576, 653
- Steidel C. C., Pettini M., Hamilton D., 1995, *AJ*, 110, 2519
- Stengler-Larrea E. A. et al. , 1995, *ApJ*, 444, 64
- Stern D. et al. , 2002, *ApJ*, 568, 71
- Vanden Berk D. E. et al. , 2001, *AJ*, 122, 549
- Yan H., Windhorst R. A., 2004, *ApJ*, 612, L93
- Zuo L., 1992, *MNRAS*, 258, 45
- Zuo L., Phinney E. S., 1993, *ApJ*, 418, 28